Proceedings of 8th International Conference on Mechanical Engineering and Renewable Energy 2025
10-12 December, 2025, Chattogram, BANGLADESH

SciEn Conference Series: Engineering Vol. 4, 2026, pp 165-170 https://doi.org/10.38032/scse.2026.4.85

Quasi-Steady Aerodynamic Modeling and Performance Analysis of an Ornithopter

Asma Azam, Sajal Chandra Banik*

Department of Mechanical Engineering, Chittagong University of Engineering & Technology, Chattogram-4349, Bangladesh

ABSTRACT

This study presents an aerodynamic analysis of an ornithopter using a quasi-steady formulation based on the Modified Strip Theory. The model incorporates key unsteady aerodynamic effects, including viscous friction, partial leading-edge suction, and dynamic stall associated with high relative angles of attack during flapping motion. The aerodynamic predictions are employed to evaluate and optimize the wing kinematics specifically the flapping frequency, forward flight speed, and pitching amplitude to achieve adequate thrust and lift for sustained flight. A comprehensive performance assessment is conducted using metrics such as lift-to-weight ratio, thrust-to-drag ratio, input power coefficient, and propulsive efficiency. The results demonstrate the capability of the modified quasi-steady model to capture the dominant aerodynamics of flapping wings while providing an effective framework for kinematic optimization and preliminary ornithopter design.

Keywords: Ornithopter, Micro Air Vehicle, Modified Strip Theory, Flapping Wing Aerodynamics, Forward Flight.

1. Introduction

The study of flapping-wing aerodynamics has progressed rapidly as researchers aim to understand and replicate the efficient flight of birds, bats, and insects. Although high-fidelity CFD can capture the complex unsteady aerodynamics of flapping wings, such simulations are computationally expensive and impractical for rapid design exploration or real-time control. Purely empirical models [1], while simple, are limited to the specific configuration from which they were derived and cannot be generalized to different ornithopter geometries or operating conditions. Consequently, physics-based analytical and numerical models have become essential tools for predicting aerodynamic forces and moments in a computationally efficient manner. These models bridge the gap between accuracy and practicality by capturing the key aerodynamic mechanisms of flapping motion without the high cost and complexity of full CFD. Existing aerodynamic approaches broadly include quasi-steady formulations, which treat aerodynamic forces as instantaneous responses to wing kinematics, and unsteady models that incorporate wake dynamics and vortex effects for greater fidelity.

The study of flapping-wing aerodynamics in forward flight originates from the seminal analyses of Theodorsen [2] and Garrick [3], who established linear potential-theory formulations for lift and thrust of a two-dimensional flapping airfoil. Subsequent developments, notably DeLaurier's [4] Modified Strip Theory, extended these foundations to large-amplitude kinematics, while later refinements by Kim et al. [5] incorporated nonlinear effects such as high angles of attack and dynamic stall. More recent work has enhanced Garrick's thrust prediction through vortical impulse theory [6], enabling representation of the complete unsteady vorticity field. These theoretical models, initially formulated for 2D airfoils, have since been generalized to finite wings for improved aerodynamic fidelity [7,8].

In this study, a computational aerodynamic framework grounded in the Modified Strip Theory is utilized to capture the effects of high relative angles of attack and dynamic stall phenomena arising from the coupled pitching and plunging motions of the wing. The resulting unsteady aerodynamic model is subsequently validated through comparison with experimental data obtained from a rigid wing subjected to prescribed heaving and pitching kinematics.

2. Aerodynamic model

To study the complex and changing nature of flapping flight, this paper uses DeLaurier's 1993 aerodynamic model. In this method, the wing is split into several strips along its span, and each strip is treated like a small airfoil. These strips are assumed to be part of a semi-elliptical wing with the same aspect ratio and flapping motion as the real wing.

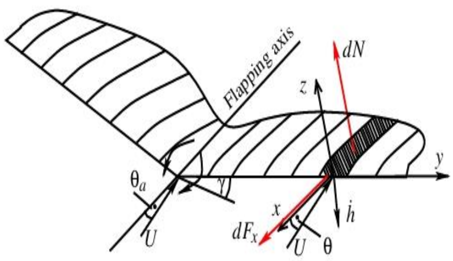

Fig. 1 Root-flapping wing [9].

2.1 Flapping Wing Kinematics

The wing's leading-edge acts as a rigid axis for spanwise twist, defined as a function of position y and time. The wing is divided into segments, each treated independently.

In the local coordinate system, the x-axis follows the chord, and the y-axis spans the wing. Each segment moves with a plunging velocity $\dot{h}$ and a pitch angle θ. The plunging displacement is given by

$$h(t) = \beta y = \beta_o y \sin(\omega t) \quad (1)$$

where β_o is the peak flapping angle. The pitch angle (θ) combines the body pitch (θ_a), wing pitch (θ_w) and a time-varying wing twist ($\delta\theta$).

$$\theta(t) = \theta_w + \theta_a + \delta\theta(t) \quad (2)$$
$$\delta\theta(t) = \theta_o y \sin(\omega t + \varphi) \quad (3)$$

and θ_o is the twist rate along the spanwise direction. The sum of body's pitch angle (θ_a) and wing's pitch angle (θ_w) defines the mean pitch angle ($\bar{\theta}$).

The angle of attack α, measured at the 3/4 chord point, describes how the wing is oriented relative to the airflow caused by its motion. It acts as the effective geometric angle of attack, accounting for plunging, pitching, and forward motion of the wing. It can be expressed as

$$\alpha = \frac{\dot{h}\cos(\theta-\theta_a) + \frac{3c}{4}\dot{\theta} + U(\theta-\bar{\theta})}{U} \quad (4)$$

2.2 Force calculation

Because the flow is unsteady, the AOA at the 3/4 chord point needs correction. The adjusted angle α′, accounts for effects like wake dynamics and downwash.

$$\alpha' = \left[C'_{Jones}(k)\alpha\right] - \frac{w_o}{U} \quad (5)$$

The unsteady wake is captured using the Finite-aspect-ratio correction to the classical Theodorsen function, denoted as $C'_{Jones}(k)$. For easier analysis, Scherer [10] provides a more convenient formulation of this function.

$$C'_{Jones}(k) = \frac{AR}{(2+AR)} C'(k) \quad (6)$$

Here, C'(k) is a complex function of the reduced frequency k, representing unsteady aerodynamic effects and expressed as $C'(k) = F'(k) + iG'(k)$. where F'(k) is the real part and G'(k) is the imaginary part of the function, capturing the in-phase and out-of-phase aerodynamic responses, respectively.

$$F'(k) = 1 - \frac{C_1 . k^2}{k^2 + {C_2}^2} \quad (7)$$
$$G(k) = -\frac{C_1 . C_2 . k}{k^2 + {C_2}^2} \quad (8)$$
$$k = \frac{\omega c}{2U} \quad (9)$$

C_1 and C_2 are given by:

$$C_1 = \frac{0.5\,AR}{(2.32+AR)} \quad (10)$$
$$C_2 = 0.181 + \frac{0.772}{AR} \quad (11)$$

Since flapping motion is harmonic, the relative angle of attack also varies periodically at the same frequency.

$$\alpha = Ae^{i\omega t} \quad (12)$$
$$\dot{\alpha} = Ai\omega e^{i\omega t} \quad (13)$$

So, the flow's relative angle of attack can be written as

$$\alpha' = \frac{AR}{(2+AR)}\left[F'(k)\alpha + \frac{c}{2U}\frac{G'(k)}{k}\dot{\alpha}\right] - \frac{w_o}{U} \quad (14)$$

The downwash term is taken from Kuethe and Chow [11] to correct the effective angle of attack.

$$\frac{w_o}{U} = \frac{2(\alpha_o + \bar{\theta})}{2+AR} \quad (15)$$

where α_o denotes the orientation corresponding to zero aerodynamic lift.

To address conditions involving high angles of attack, Kim et al. [5] introduced improvements to the MST model. In this formulation, the relative angle of attack is computed by integrating the horizontal and vertical flow velocities evaluated at the quarter-chord point along the airfoil.

$$\tau = \tan^{-1}\left(\frac{\dot{h}\cos(\theta-\theta_a) - \frac{w_o}{U} + \frac{c}{4}\dot{\theta} + U\sin\theta}{U\cos\theta - \dot{h}\sin(\theta-\theta_a)}\right) \quad (16)$$

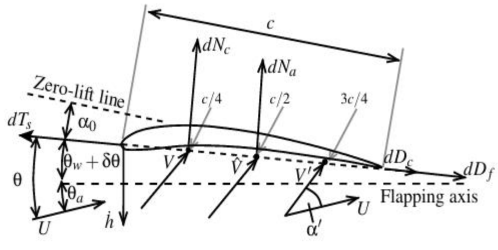

Fig. 2 Analyzed wing section with defined forces, angles, and velocities [9].

Due to the flow's unsteady nature, aerodynamic forces act at different chordwise locations, making it essential to first examine the velocity distribution across the wing. From Fig. 2, the tangential and normal flow velocities at the mid-chord location are given by:

$$V_x = U\cos\theta - \dot{h}\sin(\theta-\theta_a) \quad (17)$$
$$V_n = U\sin\theta + \dot{h}\cos(\theta-\theta_a) + \frac{c}{2}\dot{\theta} \quad (18)$$
$$\hat{V} = \sqrt{Vx^2 + Vn^2} \quad (19)$$

At the quarter-chord, the tangential velocity remains the same, but the normal component includes both the wing's motion and downwash effects, since the aerodynamic center of a cambered airfoil lies at this point.

$$V_x = U\cos\theta - \dot{h}\sin(\theta-\theta_a) \quad (20)$$
$$V_{nc} = U(\alpha' + \bar{\theta}) - \frac{c\dot{\theta}}{2} \quad (21)$$
$$V = \sqrt{Vx^2 + Vnc^2} \quad (22)$$

Figure 2 shows aerodynamic forces on a wing section, split into chordwise (x) and normal (z) components. Each segment operates in either attached or separated flow, depending on the leading-edge angle of attack.

Prouty [12] showed that for a pitching airfoil, flow can stay attached even beyond the static stall angle. This supports the use of strip theory to approximate local post-stall behavior. The dynamic stall angle from Prouty is given as:

$$\alpha_{stall} = (\alpha_{stall})_{static} + \xi\left[\frac{c\dot{\alpha}}{2U}\right]^{\frac{1}{2}} \quad (23)$$

The condition for attached flow over the wing section

$$(\alpha_{stall})_{min} \leq \left[\tau - \frac{3}{4}\left(\frac{c\dot{\theta}}{U}\right)\right] \leq (\alpha_{stall})_{max} \quad (24)$$

2.2.1 Computation of the Normal Force

The normal force (dN) acting on each section is

$$dN = \begin{cases} dN_c + dN_a & attached\ flow \\ (dN_c)_{sep} + (dN_a)_{sep} & seperated\ flow \end{cases} \quad (25)$$

Here dNc and dNa are the normal forces from circulation and apparent mass, respectively, with "sep" indicating separated flow. Under attached flow conditions, the circulatory force is characterized by the aerodynamic contribution arising from bound circulation around the airfoil.

$$dN_c = \frac{\rho UV}{2} C_n(y) \cos\tau \, cdy \quad (26)$$

Cn(y) represents the normal force coefficient, and c is the chord length at that spanwise location. Based on potential flow theory,

$$C_n(y) = 2\pi(\alpha' + \alpha_o + \bar{\theta}) \quad (27)$$

While the airfoil undergoes oscillation, the surrounding fluid accelerates, generating a reactive inertial force known as the apparent mass force. This force acts normal to the surface and is evaluated at the half-chord location, accounting for the added mass effect due to unsteady motion.

$$dN_a = \frac{\rho\pi c^2}{4} \dot{V}_n dy \quad (28)$$

where $\dot{V}_n$ is the linearized rate of change of (Vn), the mid-chord normal velocity component of ($\hat{V}$).

$$\dot{V}_n = U\dot{\alpha} - \frac{1}{4} c\ddot{\theta} \quad (29)$$

Under separated flow conditions, the wing element is treated as a bluff body; therefore, simplified force models are applied.

$$(dN_c)_{sep} = (C_d)_{cf} \frac{\rho\hat{V}.V_n}{2} cdy \quad (30)$$

The crossflow drag coefficient $(C_d)_{cf}$ used as the stall normal-force coefficient, is set to 1.98 per Hoerner [13]. In separated flow conditions, the apparent-mass force is approximated as fifty percent of its value under attached flow.

$$(dN_a)_{sep} = \frac{1}{2} dN_a \quad (31)$$

2.2.2 Chordwise Force Calculation

The total force in the x-direction on a blade element is expressed as

$$dF_x = \begin{cases} dT_s - dD_c - dD_f & attached\ flow \\ 0 & seperated\ flow \end{cases} \quad (32)$$

Here dT_s is the leading-edge suction force, dD_c the camber-induced force, and dD_f the skin friction force. The suction force arises from sharp flow diversion at the leading edge.

$$dT_s = \eta_s . 2\pi \left(\alpha' + \bar{\theta} - \frac{c\dot{\theta}}{4U}\right) \sin\tau \frac{\rho UV}{2} cdy \quad (33)$$

The efficiency factor η_s accounts for viscous effects that reduce dT_s from its potential-flow value. The camber induced drag is then estimated using potential-flow theory.

$$dD_c = -2\pi\alpha_o(\alpha' + \bar{\theta}) \cos\tau \frac{\rho UV}{2} cdy \quad (34)$$

Skin friction drag is determined by the shear forces acting along the surface of the body.

$$dD_f = \frac{1}{2}\rho {V_x}^2 (C_{df}) cdy \quad (35)$$

The skin friction drag coefficient C_{df} is given by Hoerner [13] and it varies with the Reynolds number Re, calculated using the local chord length as the characteristic dimension.

$$C_{df} = \frac{0.89}{[\log Re]^{2.58}} \quad (36)$$

2.2.3 Lift and Thrust

The expressions describing the instantaneous lift (dL) and net thrust (dT) generated by the wing section are formulated as follows.

$$dL = (dN \cos\theta + dF_x \sin\theta) \cos\gamma \quad (37)$$
$$dT = dF_x \cos\theta - dN \sin\theta \quad (38)$$

The time varying lift dL and thrust dT on each blade element defined with respect to its dihedral angle γ as shown in Fig. 1 are computed using equations (37) and (38). These are integrated spanwise to obtain total wing forces. To determine the net mean lift L and thrust T over a wingbeat cycle, the instantaneous aerodynamic forces are averaged across all sections and time steps.

2.2.4 Energy Consumption and Thrust Efficiency

The power input necessary to overcome aerodynamic forces during attached flow is formulated as:

$$dP_{in} = dF_x \dot{h} \sin(\theta - \theta_a) + dN \left[\dot{h}\cos(\theta - \theta_a) + \frac{c\dot{\theta}}{4}\right] + dN_a \left[\frac{c\dot{\theta}}{4}\right] - dM_{ac}\dot{\theta} - dM_a\dot{\theta} \quad (39)$$

The pitching moment dM_{ac} about the aerodynamic center depends on the airfoil's geometry and properties. The term dM_a accounts for contributions from apparent camber and apparent inertia, and is expressed as:

$$dM_a = -\left[\frac{1}{16}\rho\pi c^3 \dot{\theta} U + \frac{1}{128}\rho\pi c^4 \ddot{\theta}\right] dy \quad (40)$$

For separated flow, equation (39) simplifies by neglecting dF_x, dM_{ac} and dM_a resulting in a reduced expression focused solely on dominant normal-force contributions.

$$dP_{in} = dN_{sep} \left[\dot{h}\cos(\theta - \theta_a) + \frac{c\dot{\theta}}{2}\right] \quad (41)$$

The total mechanical power required consists of both inertial and aerodynamic components, accounting for the energy needed to overcome the wing's mass acceleration and aerodynamic forces during motion.

$$P_{mechanical} = P_{inertia} + P_{aero} \quad (42)$$

Inertial power comprises two components: (P_β) for rotation about the x-axis and (P_θ) for rotation about the y-axis, based on the prescribed kinematics. The total inertial power is the sum of these two contributions.

$$P_{inertial} = P_\beta + P_\theta \tag{43}$$
$$P_\beta = I_x \dot{\beta} \ddot{\beta} \tag{44}$$
$$P_\theta = 2\int_0^{\frac{b}{2}} I'_y(y)\dot{\theta}(y)\ddot{\theta}(y)dy \tag{45}$$

The moment of inertia of the entire wing about the x-axis through the fulcrum is denoted by I_x while I'_y represents that of an individual section about its spanwise centroidal axis. Their expressions are as follows.

$$I_x = 2\rho_\omega t\int_0^{\frac{b}{2}} c(y)y^2dy \tag{46}$$
$$I'_y(y) = \frac{\rho_\omega t c^3(y)}{12} \tag{47}$$

With ρ_ω as the wing material density and t as its thickness, the rotational power P_θ about the y-axis is expressed as:

$$P_\theta = \frac{\rho t {\theta_o}^2\omega^3 \sin 2(\omega t+\varphi)}{12}\int_0^{\frac{b}{2}} c^3(y)y^2dy \tag{48}$$

The wing's instantaneous aerodynamic power is calculated by integrating forces along the span, while the mean input power over a flapping cycle is derived through time-averaging. Given a constant flight velocity U, the mean aerodynamic output power is computed as the product of average thrust and flight speed.

$$\bar{P}_{out} = \bar{T}U \tag{49}$$
$$\bar{\eta} = \frac{\bar{P}_{out}}{\bar{P}_{in}} \tag{50}$$

To avoid nonphysical outcomes in kinematic optimization, it is essential to account for both elastic energy storage and the dissipation cost associated with negative mechanical power. Following the approach proposed by Kurdi et al. [14], the mechanical power can be reformulated to include these effects:

$$P_{\text{mech}} = \begin{cases} -\alpha_e \mid P_{\text{mech}} \mid +\beta_e(1-\alpha_e) \mid P_{\text{mech}} \mid, & \text{if } P_{\text{mech}} < 0 \\ P_{\text{mech}}, & \text{if } P_{\text{mech}} \geq 0 \end{cases}$$

Here, α_e represents the fraction of negative power that is elastically stored, while β_e denotes the proportion of the remaining power that is dissipated. These parameters range between 0 and 1, with the following interpretations:

$\alpha_e = 0$ no elastic recovery
$\alpha_e = 1$ full elastic recovery
$\beta_e = 0$ no dissipation cost
$\beta_e = 1$ full dissipation cost

This formulation ensures a more realistic representation of mechanical power, especially under conditions where negative power arises due to unsteady aerodynamic loading. In this study, both parameters were set to zero ($\alpha_e = 0, \beta_e = 0$) to exclude elastic storage and dissipation effects, allowing a direct evaluation of the aerodynamic power requirements.

3. Result validation

To evaluate the accuracy of the proposed aerodynamic model, a comparative analysis was conducted against the experimental data presented by Okamoto and Azuma [15] for a flat plate with a sharp leading edge undergoing combined heaving and feathering motion. The simulation was configured to match the experimental conditions: Reynolds number $Re = 8.0 \times 10^3$, heaving amplitude ratio $h_1/c = 0.68$, reduced frequency $k = 0.32$, phase shift $\psi_\theta = -93°$, and feathering amplitude $\theta_1 = 6.7°$.

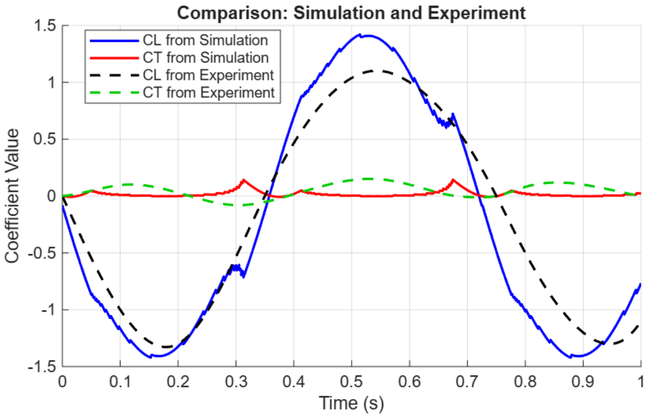

Fig. 3 Comparisons of aerodynamic coefficients between experiment and analysis.

Figure 3 illustrates the time histories of the perpendicular force coefficient $C_L$and thrust coefficient C_T, comparing simulation results with digitized experimental data. The predicted lift coefficient C_L aligns well with experimental trends, capturing key peaks and phase timing. Minor simulation fluctuations stem from dynamic stall during rapid unsteady motion, causing transient flow separation. The thrust coefficient (C_T) shows a consistent mean value with the experiment, while the detailed harmonic waveform differs due to unsteady vortex-dominated effects not fully captured by the quasi-steady model. Positive mean thrust is accurately reproduced, confirming the model's handling of lift-tilt and drag effects.

4. Kinematic optimization

A multi-variable optimization of wing kinematics was conducted to enhance the aerodynamic performance of the flapping-wing ornithopter. The goal was to maximize average thrust while ensuring average lift exceeded body weight ($\bar{L}$ > W). A constraint on propulsive efficiency (0 < $\bar{\eta}$ <1) ensured physically realistic power use. Six key parameters were optimized: flapping frequency (f), flight speed (U), plunge amplitude (β_0), pitch amplitude (θ_0), mean incidence (θ_a), and phase lag (φ). Parameter bounds were based on biological flyers and prior experiments. The optimization problem was cast as a constrained nonlinear program and addressed using MATLAB's *fmincon* solver with the Sequential Quadratic Programming (SQP) algorithm. The cost function minimized negative thrust, converting the maximization into a minimization task. Penalty terms discouraged solutions violating lift or efficiency constraints to ensure feasible, high-performance outcomes.

Table 1 Ornithopter properties

Wingspan	0.4m
Root chord	0.08m
Aspect ratio	6.4
Weight	40 grams

Table 2 Aerodynamic data for Liebeck LPT airfoil [16]

Symbol	Description	Value
α_o	Angle of sections zero Lift line	0.5 (Deg)
η_s	Leading edge suction efficiency	0.98
C_{mac}	Moment coefficient about aerodynamic center	0.025
$(\alpha_{stall})_{max}$	Airfoil's stall angle	13 (Deg)

Table 3 Initial guesses, bounds for design optimization and optimum value

Variable	Initial guess	Lower Bound	Upper Bound	Optimum value
f (Hz)	2.5	0.5	10	4
U(m/s)	5	2	15	7
β_o (deg)	20	10	50	30
θ_o (deg)	20	10	50	33
θ_a (deg)	2	2	15	4
φ (deg)	0	-90	90	90

5. Parametric influence on flight performance

Figures 4–7 illustrate the variation in key performance metrics including lift-to-weight ratio, thrust-to-drag ratio, power coefficient, and propulsive efficiency as functions of the primary kinematic parameters: flapping frequency, flapping amplitude, dynamic twist, and mean pitch angle. The red dot in each subplot marks the optimized design point identified through the kinematic optimization process.

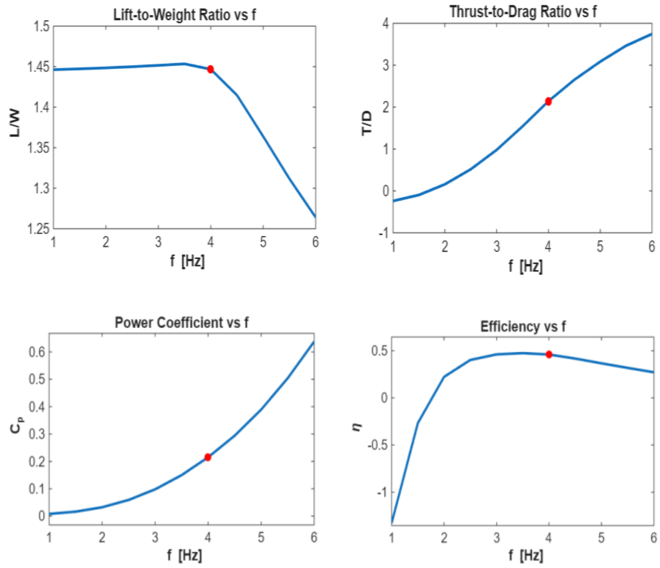

Fig. 4 Frequency variation

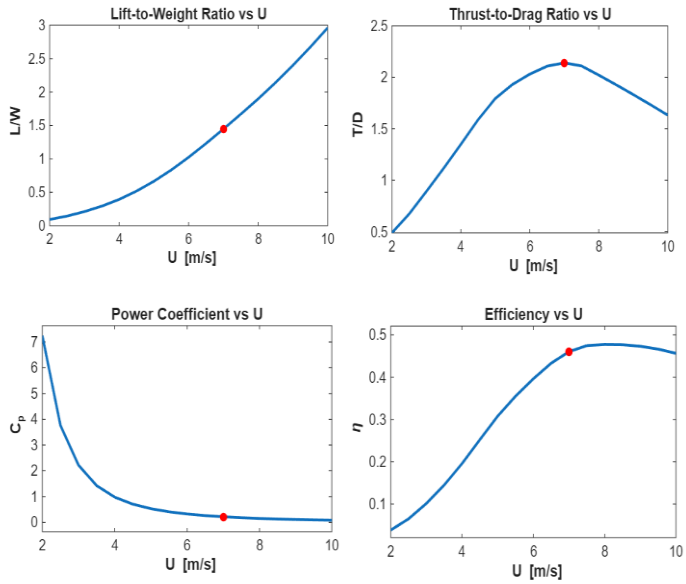

Fig. 5 Forward speed variation

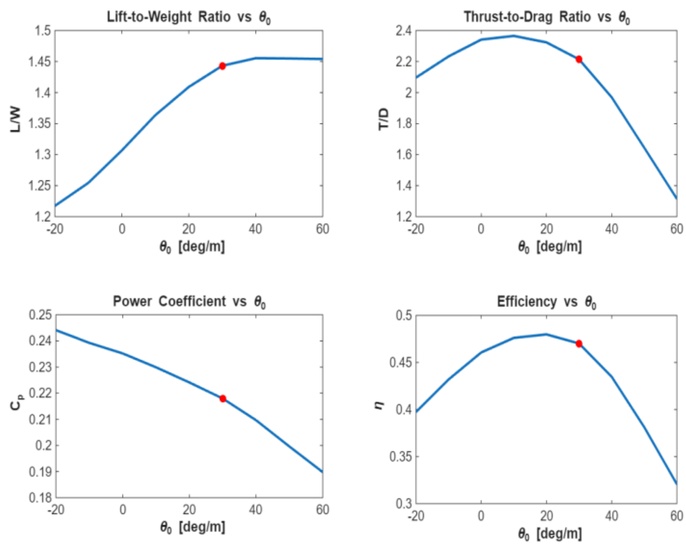

Fig. 6 Dynamic twist angle variation

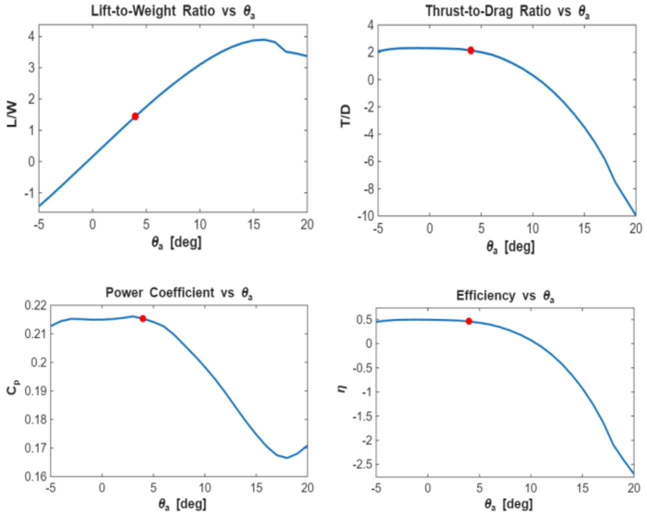

Fig. 7 Mean pitch angle variation

6. Conclusion

In conclusion, this research successfully developed a comprehensive aerodynamic and kinematic analysis framework for a 40 cm wingspan, 8 cm root chord ornithopter, leveraging a quasi-steady aerodynamic model originally proposed by DeLaurier. Through kinematic optimization, the study identified optimal flapping parameters that ensure lift generation exceeding the ornithopter's weight while maintaining realistic and practical propulsive efficiency. Unlike classical unsteady aerodynamic models, the employed approach integrates critical viscous friction effects, partial leading-edge suction, and accurate post-stall flow behavior, thereby providing a more realistic depiction of the aerodynamic environment encountered during flapping flight. Moreover, the model captures both inertial and aerodynamic forces, enabling a holistic understanding of the system dynamics. Overall, the methodology and findings presented here contribute significantly to the design and optimization of bio-inspired flapping wing vehicles by balancing aerodynamic performance with practical constraints.

References

[1] J. Grauer, E. Ulrich, J. Hubbard, D. Pines, and J. S. Humbert, "Testing and System Identification of an Ornithopter in Longitudinal Flight," *J. Aircraft*, vol. 48, no. 2, pp. 660–667, Mar. 2011.

[2] T. Theodorsen, "General Theory of Aerodynamic Instability and the Mechanism of Flutter," NACA-TR-496, Jan. 1949.

[3] I. E. Garrick, "Propulsion of a flapping and oscillating airfoil." Jan. 01, 1937.

[4] DeLaurier, J.D., "An Aerodynamic Model for Flapping Wing Flight," *Aeronaut. J. R. Aeronaut. Soc.*, pp. 125–130, Apr. 1993.

[5] D. K. Kim, J. S. Lee, J. Y. Lee, and J. H. Han, "An aeroelastic analysis of a flexible flapping wing using modified strip theory," in *Active and Passive Smart Structures and Integrated Systems 2008*.

[6] R. Fernandez-Feria, "Linearized propulsion theory of flapping airfoils revisited," *Phys. Rev. Fluids*, vol. 1, no. 8, p. 084502, Dec. 2016.

[7] F. Ayancik, Q. Zhong, D. B. Quinn, A. Brandes, H. Bart-Smith, and K. W. Moored, "Scaling laws for the propulsive performance of three-dimensional pitching propulsors," *J. Fluid Mech.*, vol. 871, pp. 1117–1138, Jul. 2019.

[8] A. J. Smits, "Undulatory and oscillatory swimming," *J. Fluid Mech.*, vol. 874, p. P1, Sep. 2019.

[9] S. M. H. A. Valiyff, J. R. Harvey, M. B. Jones and J. L. Palmer, "Analysis of Ornithopter-Wing Aerodynamics," presented at the 17th Australasian Fluid Mechanics Conference, Auckland, New Zealand, Dec. 2010.

[10] J Otto Scherer., "Experimental and theoretical investigation of large amplitude oscillation foil propulsion systems.," HYDRONAUTICS INC. LAUREL MD, Technical report, 1968.

[11] A. M. Kuethe and C.-Y. Chow, *Foundations of Aerodynamics: Bases of Aerodynamic Design*. John Wiley & Sons, 1997.

[12] R. W. Prouty, *Helicopter Performance, Stability, and Control*. R.E. Krieger Publishing Company, 1995.

[13] Sighard F Hoerner, *Fluid-Dynamic Drag*.

[14] M. Kurdi, B. Stanford, and P. Beran, "Kinematic Optimization of Insect Flight for Minimum Mechanical Power," Jan. 2010.

[15] M. Okamoto and A. Azuma, "Experimental Study on Aerodynamic Characteristics of Unsteady Wings at Low Reynolds Number," *AIAA J.*, vol. 43, no. 12, pp. 2526–2536, 2005.

[16] M. Zakaria and Amgad M. Bayoumy-Aly, "Numerical Aerodynamic Characteristics of Flapping Wings," *Int. Conf. Aerospace Sci. Aviat. Technol.*, May 2009.